Sixth International Symposium on Marine Propulsors
smp'19, Rome, Italy, May 2019

Towing Tank Model Tests for Propulsive Performance Analysis of a Waterjet Propelled Amphibious Vehicle

Jeonghwa Seo[1], Hoe-seong Jeong[2], Kyogun Chang[3], Jongyeol Park[4], Shin Hyung Rhee[4,5]

[1]Dept. of Naval Architecture and Ocean Engineering, Chungnam University, Daejeon, Korea
[2]Naval Force Analysis, Test & Evaluation Group, Republic of Korea Navy, Gyeryong, Korea
[3]Agency for Defense Development, Daejeon, Korea
[4]Dept. of Naval Architecture and Ocean Engineering, Seoul National University, Seoul, Korea
[5]Research Institute of Marine Systems Engineering, Seoul National University, Seoul, Korea

ABSTRACT

The present study aims to examine the resistance and propulsion performance of an amphibious vehicle with waterjet propulsion by conducting a series of towing tank model tests. The test model was an armored vehicle consisted of a box-shaped chassis, two flush-type waterjets, a bow flap, and a trimtab. Following the powering prediction procedure of a conventional ship, the resistance test, waterjet system and bollard pull test, and self-propulsion test were performed. The Froude number based on the characteristic length and advance speed for the model test ranged from 0.883 to 1.275. The effect of the track deployment conditions was also investigated by conducting a test with the retracted and normal track condition. In the bollard pull and self-propulsion test where two waterjets were installed onto the chassis, the flow rate of the waterjet was higher than that in the single waterjet system test, resulting in high thrust. The propulsive efficiency increased in high advance speeds as the transom was exposed to air.

Keywords

Waterjet, Model Test, Towing Tank, Self-propulsion test

1 INTRODUCTION

Waterjet propulsion systems have been widely used in marine vessels, thanks to its advantages of low cavitation in high loading, safe operation in shallow water, and good maneuverability in low advance speed (Allison, 1993).

The main concern of the test design for waterjet propulsive performance is how to measure the flow rate accurately. The flow rate determines the momentum flux or gross thrust at the nozzle end. Direct measurement of the flow velocity distribution or the volume rate at the waterjet nozzle is the simplest way (Jung et al., 2009), but it is difficult to achieve the test setup for such flow measurement if the test model continuously changes its running attitude.

The flow rate could be also indirectly estimated by measuring the net thrust or momentum flux of the waterjet system. A bollard pull test which measures the net force on the vessel in zero advance speed is a method for the estimation of the flow rate (Kim et al., 2009) from the gross thrust.

Examples of waterjet propulsion mostly deal with planing hulls, but waterjets have been also used for different types of marine vehicles. Amphibious armored vehicles are a unique application of waterjet propulsion systems. Although the target speed is not as high as the high-speed vessels and the expected efficiency is considerably low, waterjet propulsion is the most feasible option for such vehicles. The propulsive characteristics of waterjet propulsion are similar to generic high-speed vessels, but the propulsor and hull interaction must be significantly different owing to the large draft and severe flow separation at the transom (Lee et al., 2017).

The present study aims to understand the propulsive characteristics of an amphibious vehicle by conducting a series of model tests in a towing tank. Focusing on the flow rate, the waterjet performance was investigated by waterjet system tests, bollard pull tests, and self-propulsion tests. The running attitude changes by the waterjet in various operating conditions were also examined.

2 TEST SETUP

2.1 Test model

A scaled model of an amphibious vehicle was used in the present study. Figure 1 shows the vehicle model, which consisted of the chassis body (hull), tracks, a bow flap, and a trimtab, representing the typical arrangement of an

amphibious vehicle. The waterline length, width, and draft of the hull were 2.506*Lc*, 1.058*Lc*, and 0.4718*Lc*, respectively, where L_C is the characteristic length of the vehicle, which is defined as the cubic root of the model displacement. The vertical distance from the hull to the track bottom was 0.125*Lc*

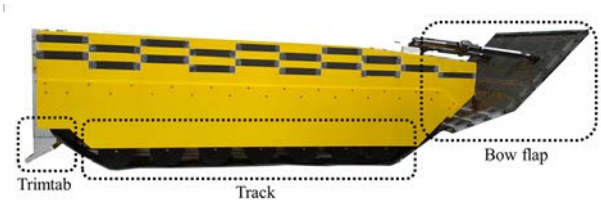

Figure 1. Hull of the test model (top) and fully-appended test model (bottom)

The bow flap was designed to produce lift force on the hull. The incidence angle and length of the bow flap's lower part was 20° and 0.657*Lc*, respectively. The trimtab had the incidence angle of 30° to generate lift force at the stern. The chord length of the trimtab was 0.153*Lc*.

Figure 2 shows the design of the waterjet model. Two waterjets were made to be fit to the vehicle model. The waterjet consisted of the intake, a seven-bladed impeller, a six-bladed stator, pump casing, and a converging nozzle. The diameter of the impeller, *D*, was 0.1834*Lc*. The diameter of the nozzle outlet was 0.73*D* and the impeller axis was 0.80*D* above the hull bottom.

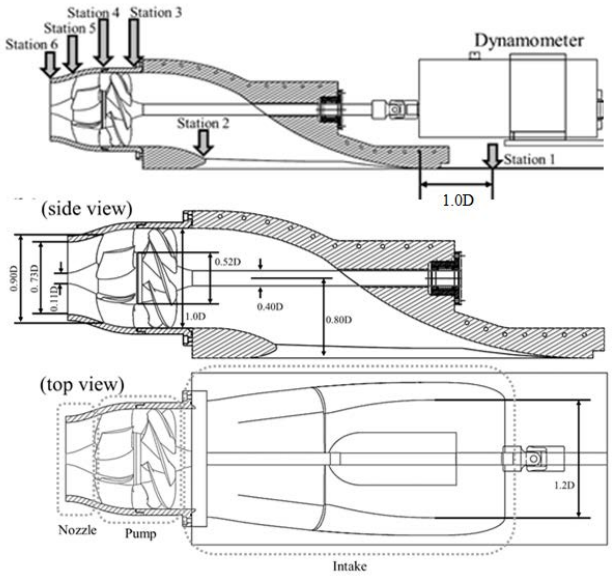

Figure 2. Schematic of the waterjet model

2.2 Test conditions

Waterjet System Tests (ITTC, 2017), WST in short, were conducted prior to the tests with the vehicle model. WST, which corresponds to the propeller open water tests for screw propellers, refers to model test with the whole waterjet system that consists of the intake, pump, and nozzle.

WST was conducted to measure the waterjet nozzle exit flow rate in a fixed running attitude. Note that the same flow rate could not be measured in bollard pull tests (BPT) and self-propulsion tests (SPT), where the running attitude kept changing dynamically. The flow rate measurement results were used to estimate the net thrust and the waterjet and hull interaction.

The waterjet was installed to a dummy hull, designed to lead the fully developed turbulent boundary layer into the intake. Figure 3 shows the design of the dummy hull with a vertical traverse system. The length of the dummy hull was similar to that of the vehicle model to ensure that the Reynolds numbers (*Re*) were similar.

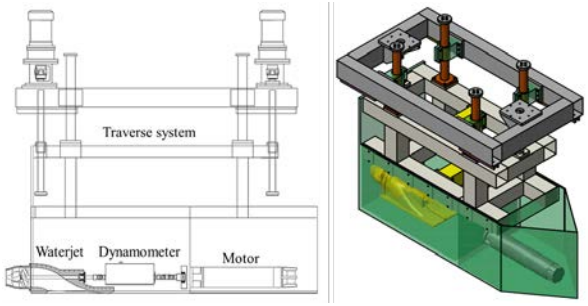

Figure 3. Schematic of the dummy hull and traverse system for WST.

Table 1 shows the test conditions for WST. WST conditions were set by changing the advance speed (*U*) and impeller revolution rate (*n*) for the advance ratio (*J*) variation. Three *U* cases were chosen: zero, 50% U_D, and 100% U_D, where U_D is the design advance speed in model scale. The corresponding Froude number (*Fr*) with 100% U_D was 0.981. The revolution rate was varied from 50% n_D to 100% n_D with the interval of 12.5% n_D, where n_D is the design revolution rate. Total 15 test conditions were selected for WST.

Table 1. Test conditions of WST

J	*n* (% n_D)	*U* (% U_D)	Re_c (×10^6)
0	50 - 100	0	1.48 – 2.46
0.236	100	50	2.47
0.262	87.5		2.22
0.295	75		2.00
0.337	62.5		1.73
0.393	50		1.49
0.471	100	100	2.49
0.524	87.5		2.25
0.589	75		2.00
0.673	62.5		1.76
0.786	50		1.52

BPT was performed with the vehicle model equipped with two waterjets. n was varied from 83.3% n_D to 113.33% n_D, while the hull was free to pitch and heave at U = 0. To validate the flow rate estimation by the WST results, the net thrusts from two waterjets were compared with the net x-directional force on the hull. The waterjet and hull interaction was also investigated by comparing WST results to those of BPT.

Table 2 shows the test conditions for resistance tests (RT) and SPT. Eight Fr conditions ranged from 0.883 to 1.275 were selected for RT. The corresponding Reynolds numbers (Re) ranged from 693,000 to 2,249,000. Both closed and open intake conditions were tested in RT, although RT with closed waterjet duct is recommended by ITTC (ITTC, 2011). For the open intake condition, the water flowed through the waterjet duct without the impeller and stator. For SPT, three Fr conditions were selected out of RT cases.

Table 2. Test condition of RT and SPT

U (%U_D)	Fr	Re ($\times 10^6$)	RT	SPT
40	0.392	0.69	O	
60	0.589	1.04	O	
80	0.785	1.38	O	
90	0.883	1.56	O	
100	0.981	1.73	O	O
110	1.079	1.90	O	O
120	1.177	2.08	O	O
130	1.275	2.25	O	

2.3 Test facility and measurement system

The model tests were performed in the Seoul National University Towing Tank. The length, width, and depth of the basin were 110 m, 8 m, and 3.5 m, respectively.

The dummy hull for WST was installed to the towing carriage by a vertical traverse system to restrain the motion of the test rig. WST was conducted in a fully immersed condition, conforming to the arrangement of the waterjet in the vehicle.

The torque and thrust of the waterjet impeller in WST, BPT, and SPT were measured by a dynamometer. The maximum measurable range of the impeller thrust (T_{imp}) and torque (q) was 1,000 N and 50 N·m, respectively.

The averaged pressure magnitudes at Stations 1, 3, 5, and 6 (p_1, p_3, p_5, and p_6) were measured by a pressure transducer, DP-15 (Validyne Engineering, Northridge, CA). To obtain the pressure of the ingested flow (p_0), to be used as the reference pressure, the pressure at Station 1 with closed intake was acquired first.

The flow rate at the nozzle exit was measured by using a laser Doppler velocimetry (LDV) system, FlowLite (Dantec Dynamics A/S, Skovlunde, Denmark). It measured longitudinal one-dimensional velocity component at 37 points behind the nozzle exit. The locations of LDV measurement are presented with the measurement results.

Figure 4 shows the test arrangement adopted for RT, BPT, and SPT. A loadcell with the maximum capacity of 2,000 N was used to measure the resistance (R) for RT and towing force (F_x) for BPT and SPT. Two-degrees-of-freedom motion of the test model, that is, pitch and heave, was allowed during the tests.

2.4 Data reduction

The data reduction process of the present study was based on the ITTC 96 method (ITTC, 1996). The purpose of the data reduction was to derive the net thrust coefficient ($K_{T,net}$), torque coefficient (K_q), and net efficiency (η_{net}) with the advance ratio (J) variation, similar to the analysis of conventional screw propellers. $K_{T,net}$ in WST was

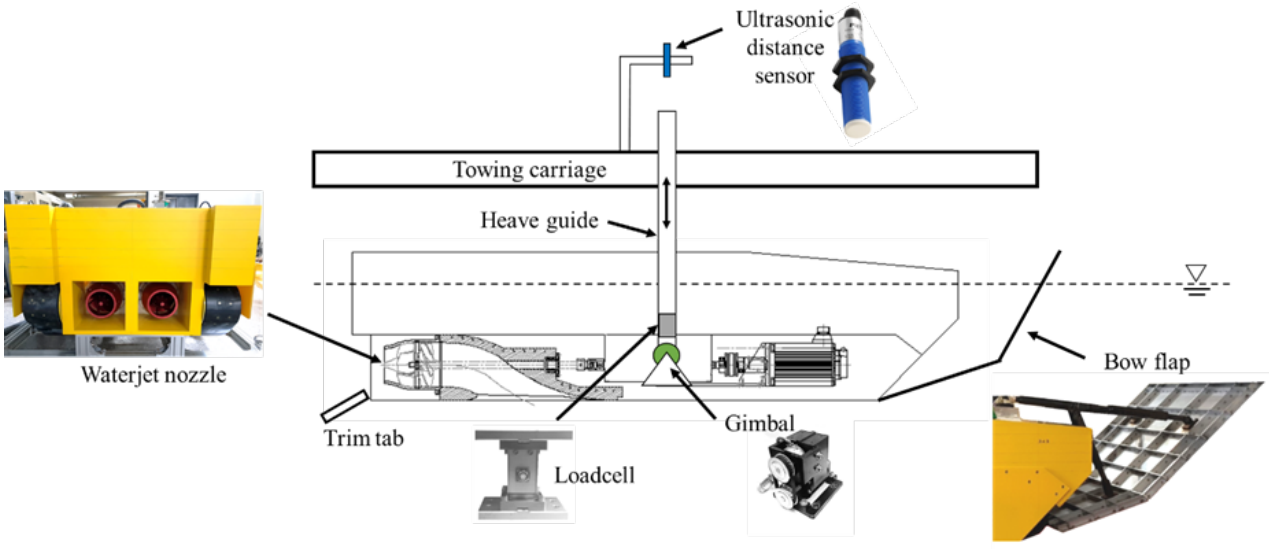

Figure 4. Test arrangement for the RT, BPT, and SPT

estimated by analyzing the momentum flux, while K_q was directly acquired from the measured torque at the impeller axis.

The flow rate (Q) estimation was the starting point of the waterjet performance analysis. Q was obtained by the following formula

$$Q = \rho A_5 A_6 \sqrt{\frac{p_5 - p_6}{0.5\rho(A_5^2 - A_6^2)}} \quad (1)$$

Because of the energy loss through the nozzle, the flow rate correction (γ) should be introduced. In the present study, γ was obtained by direct LDV measurement (γ_{LDV}). Eq. (2) shows estimation of the net thrust (T_{net}) by p and Q. T_{net} was defined as the difference between the ingested momentum flux at Station 1 (M_1) and the gross thrust, that is, the momentum flux at Station 6 (M_6). Note that the ingested momentum flux was not affected by impeller operation.

$$T_{net} = M_6 - M_{1,@n=0} = \gamma\rho Q\left(\sqrt{\left(\frac{\gamma Q}{A_6}\right)^2 + \frac{(p_6 - p_1)}{0.5\rho}} - V_{1,@n=0}\right) \quad (2)$$

The ingested momentum flux in SPT is quite complicated like conventional vessels where wake fraction (w) is taken account of. The ingested flow (U_A) is retarded, and $V_{1,@n=0}$ or UA is expressed as $U(1 - w)$.

Table 3 shows the test uncertainty analysis results, following the American Society of Mechanical Engineers (ASME) standards (ASME, 2005). The systematic uncertainty was acquired from test elements and error propagation, while the random uncertainty was obtained from tests repeated 10 times.

Table 3. Test uncertainty of the waterjet performance

	Random uncertainty	Systematic uncertainty	Total uncertainty
C_{p1}	0.000	0.002	0.004
C_{p3}	0.003	0.002	0.007
C_{p5}	0.007	0.002	0.015
C_{p6}	0.002	0.002	0.006
C_Q	0.003	0.001	0.006
K_q	0.002	0.001	0.004
$K_{T,net}$	0.005	0.003	0.012
η_{net}	0.006	0.004	0.014

3 PROPULSIVE CHARACTERISTICS OF THE WATERJET

3.1 Flow rate at U=0

Figure 5 shows the LDV measurement results at U = 0 and n = 100% n_D. The measured local axial velocity, v, was non-dimensionalized by the mean axial velocity at Station 6 (V_6). The locations of the LDV measurement are also presented in Figure 5.

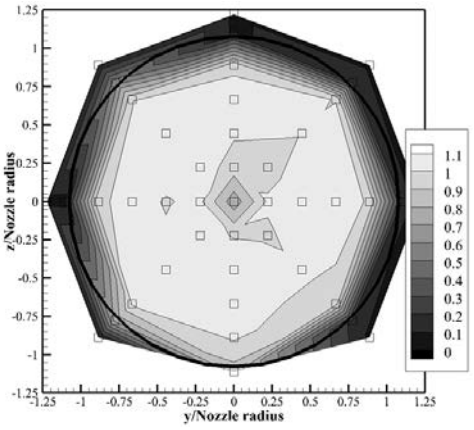

Figure 5. LDV measurement points (square symbols) and v/V_6 distribution at U = 0% U_D and n = 100% n_D.

The flow rate by LDV measurement was used to correct Q in Eq. (1), as follows.

$$Q_{LDV} = \gamma_{LDV} Q = \gamma_{LDV}\rho A_5 A_6 \sqrt{\frac{p_5 - p_6}{0.5\rho(A_5^2 - A_6^2)}} \quad (3)$$

where γ_{LDV} is the correction by LDV measurement. In the present study, γ_{LDV} was 0.8759.

3.2 Propulsive performance in WST

The propulsion performance of the waterjet system was represented as the efficiency of the power conversion from $P_D = 2\pi nq$ to $P_{net} = T_{net}U$. The input to the waterjet system, P_D, was converted to the kinetic energy flux of the flow (E_{53}) through the pump with the pump efficiency (η_{pump}). The kinetic energy reduced in the intake and nozzle, i.e., the duct system, and the residual kinetic energy (E_{61}) generated the effective work rate by $T_{net}U$ at the nozzle end. The duct efficiency (η_{duct}) was defined as the ratio of E_{61} to E_{53}, which means the input and output kinetic energy flux of the flow through the duct, respectively. The product of ηpump and ηduct is the jet system efficiency (η_{JS}). The jet efficiency (η_{jet}) denotes the efficiency in converting the kinetic energy flux into effective work by the thrust by the nozzle. η_{net} is the product of η_{pump}, η_{duct}, and η_{jet}.

$$\eta_{net} = \frac{T_{net}U}{2\pi nq} = \frac{E_{53}}{2\pi nq}\frac{E_{61}}{E_{53}}\frac{T_{net}U}{E_{61}} = \eta_{pump}\eta_{duct}\eta_{jet} = \eta_{JS}\eta_{jet} \quad (10)$$

The energy conversion process in WST was firstly investigated and then compared with the results in BPT. Figure 6 (a) shows the impeller performance results in WST. Although the impeller propeller loading represented by $K_{T,imp}$ and K_q decreases for larger J as generic marine propellers (Seo et al., 2016), the flow rate coefficient slightly increased.

Figure 6 (b) shows the pump performance in non-dimensional form: input power coefficient (K_{PD}), output kinetic energy flux coefficient (C_{E53}), and η_{pump}. As the impeller loading decreased for larger J, the input power also reduced. The output kinetic energy flux, however, increased as the flow rate, resulting in growth of η_{pump}.

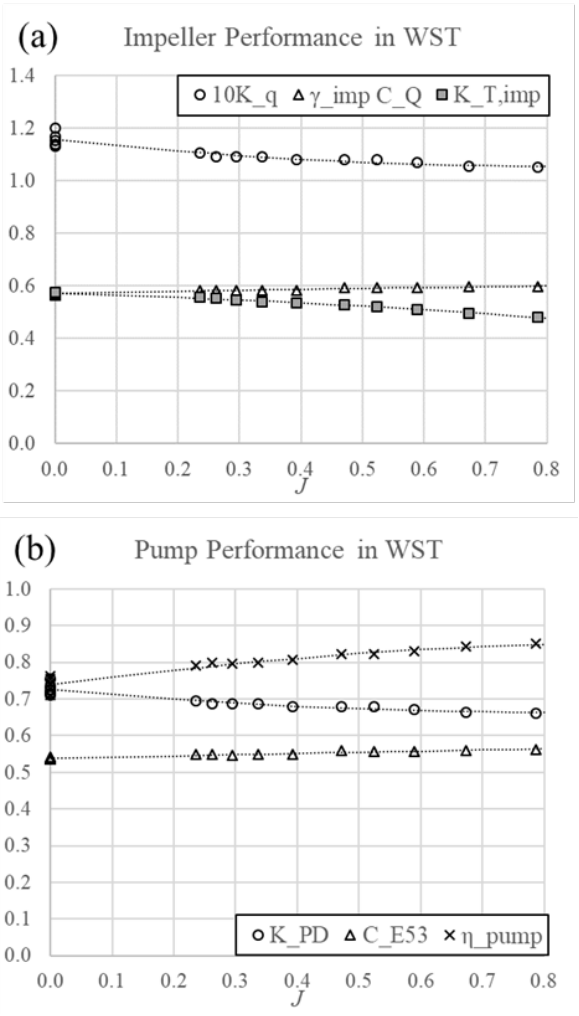

Figure 6. Impeller and pump performance in WST: (a) $K_{T,imp}$, K_Q, and $\gamma_{imp}C_Q$ with J variation and (b) K_{PD}, C_{E53}, and η_{pump} with J variation

The flow generated by the pump flows through the duct and lost its energy, and the loss at the intake and nozzle should be addressed when η_{duct} was examined.

Figure 7 (a) shows the change of the kinetic energy flux through the duct and energy loss with J variation. The energy flux of the ingested flow, E_1, was derived from U. The intake loss of the ingested flow, E_{13}/E_1, was 31% in average. For higher J, the amount of the intake loss increased as E_1 increased. The nozzle loss, E_{65}, is a function of Q, thus slightly grew for larger J. Figure 7 (b) shows the jet system efficiency. The pump efficiency shown in Figure 6 (b) increased, for larger J, but the duct efficiency reduced. The jet system efficiency, the product of η_{pump} and η_{duct}, was almost uniform.

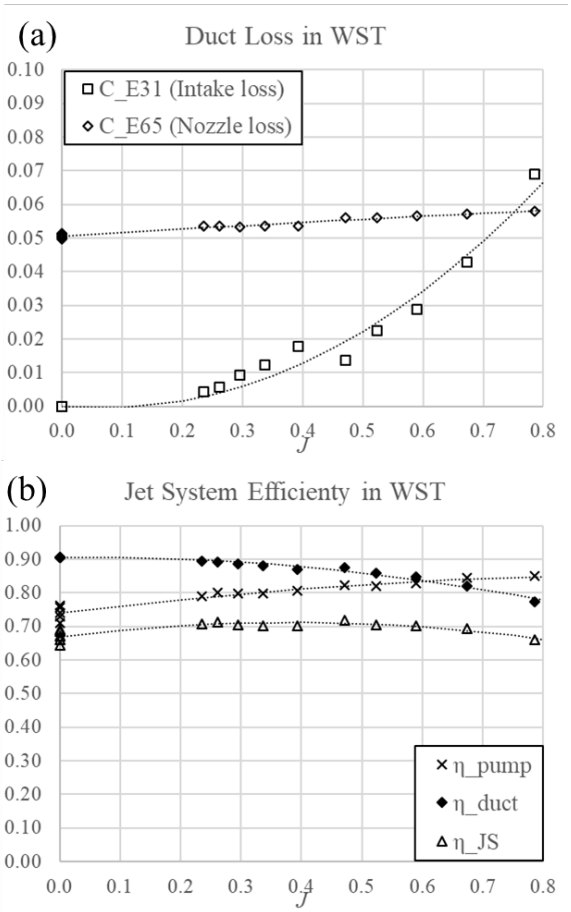

Figure 7. Changes of the energy flux through the duct and energy loss in WST with J variation: (a) intake and nozzle loss and (b) Jet system efficiency

Figure 8 shows thrust generation at the nozzle, i.e., T_{net} and energy flux conversion at the jet. When the flow with the kinetic energy flux of E_{61} leaves the nozzle exit with the momentum flux of M_{61}, the reaction force produces the thrust of T_{net}. In terms of energy conversion, E_{61} was converted into the work rate by the thrust, $T_{net}U$.

In ideal condition, pressure change through the waterjet is not considered, and p_{61} in Eq. (1) is assumed to be zero; therefore, the energy flux and momentum flux through the duct can be presented in terms of V_1 and V_6, or jet velocity ratio ($JVR = V_{1\,@\,n=0}/V6$). In actual WST results, however, the pressure should be included in the energy flux. As p_6

and C_{p6} was negative, both C_M and C_E in actual results were smaller than the ideal case.

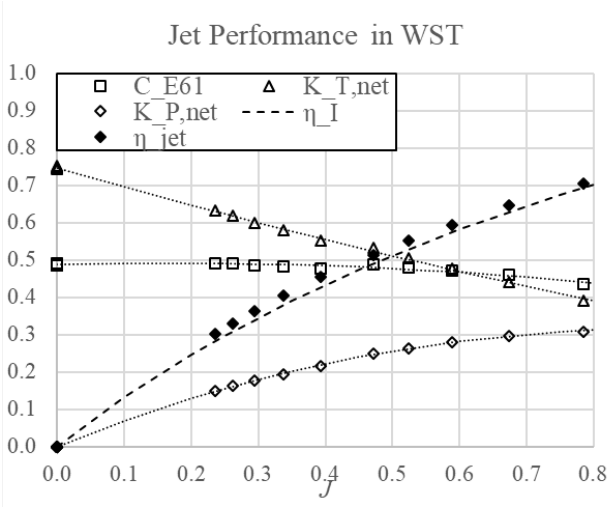

Figure 8. Jet performance in WST

Figure 9 shows the waterjet system performance. For waterjet design, to reduce the intake loss for growing η_{duct} and reduce V_6 for increasing η_I could be effective to achieve high η_{net}.

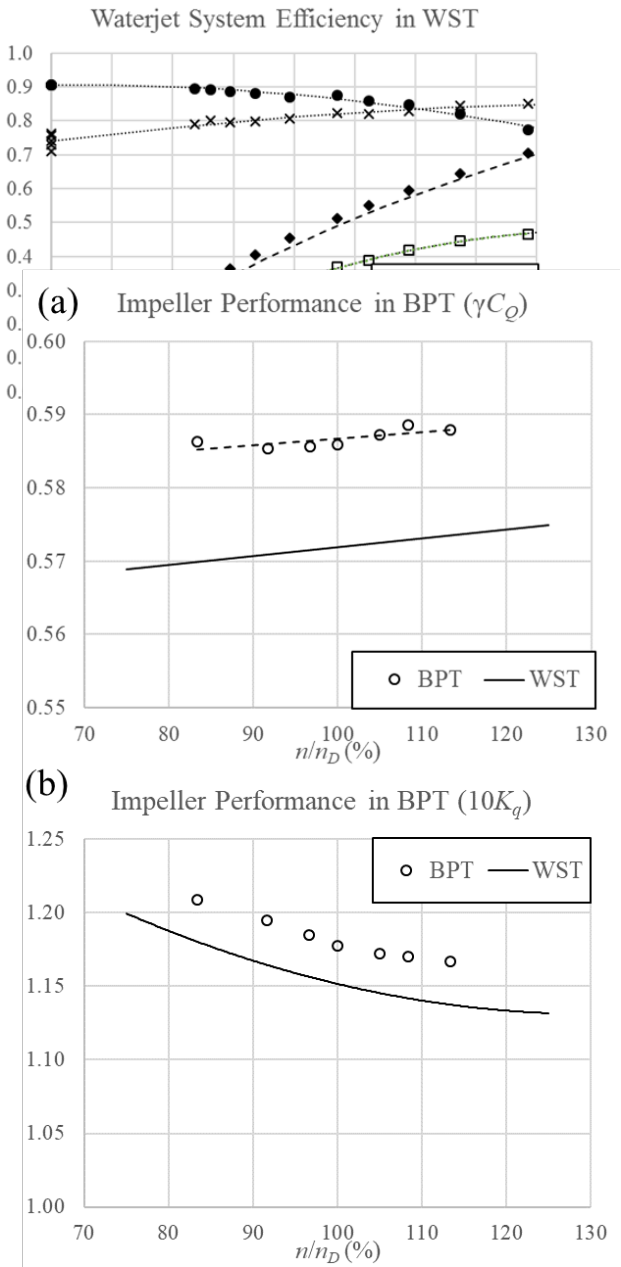

Figure 9. Waterjet system performance in WST: efficiency of energy conversion

3.3 Propulsive performance in BPT

Figure 10 shows the impeller performance and nozzle pressure in BPT and comparison with that in WST at U = 0. Two waterjets in BPT swept the flow around the transom strongly and kept the pressure at the nozzle end, i.e., p_6, lower than WST condition. Swirling flow behind the truncated transom and aeration to the nozzle exhaust flow was developed in BPT while remarkable free-surface behavior was not observed in WST. It resulted in the growth of the flow rate and impeller loading.

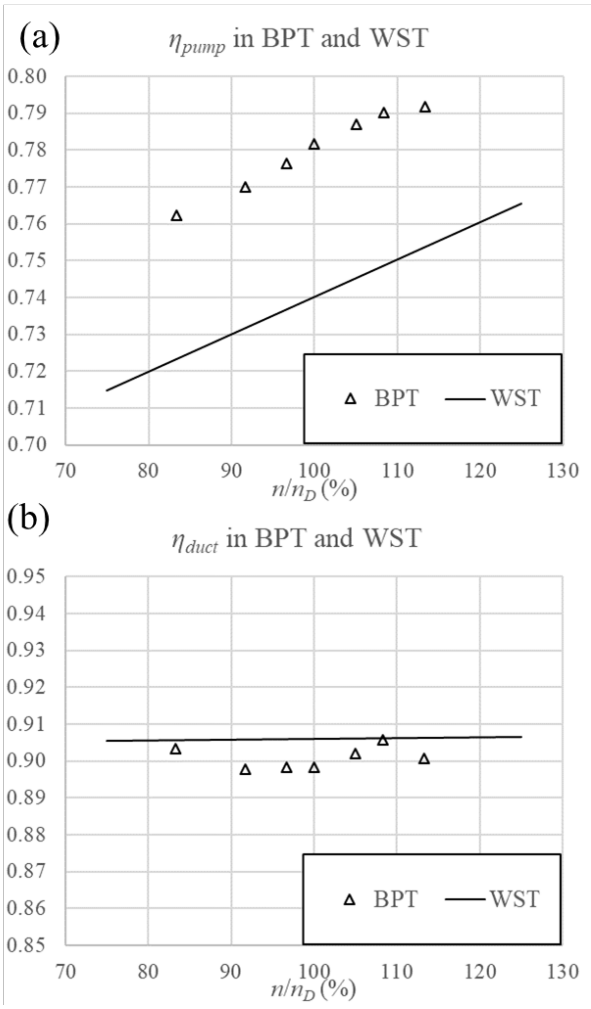

Figure 10. Impeller performance in BPT: (a) Flow rate coefficient γC_Q and (b) K_q

Figure 11 (a) and (b) shows η_{pump} and η_{duct} in BPT. η_{pump} increased in BPT as the growth of the flow rate was larger than that in the impeller torque owing to the favorable operation condition with reduced p6. The effects of free-surface behavior on the waterjet performance is discussed again in the next section of SPT results, where severe free-surface behavior was observed. Regarding η_{duct}, it reduced in BPT. Increase of the flow rate in BPT increased the energy loss through the nozzle.

4 WATERJET-HULL INTERACTION IN SPT

For SPT, the self-propulsion point in the model scale was obtained from n variation, and the surface skin friction correction between the model and full scale was not introduced. In the same manner as WST and BPT, p, T_{imp}, q, and F_x with n variation was measured. The results in three n conditions at uniform U were interpolated to the

self-propulsion point. The efficiency of the waterjet components, i.e., η_{pump}, η_{duct}, and η_{jet}, were derived from the propulsion analysis and compared with that of WST and BPT.

Figure 11. Waterjet system performance in BPT: (a) η_{pump} and (b) η_{duct}

The most important difference between WST with the dummy hull and SPT with the vehicle hull was the exposure of the nozzle end, as shown in Figure 12. In WST, the transom and nozzle of the model were fully submerged. In SPT, however, the transom was exposed to air as *Fr* increased. There was massive flow separation at the truncated tail of the model in RT, but the flow separation was swept by the waterjet exhaust in SPT, resulting in partially dry transom.

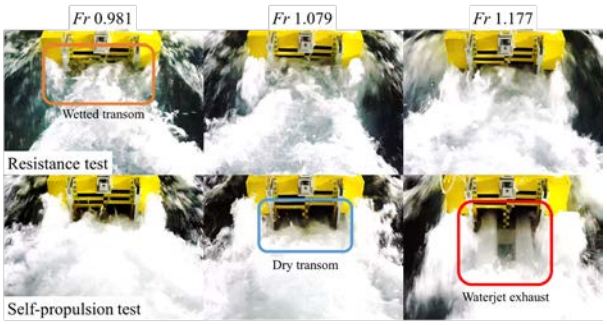

Figure 12. Snapshots of the transom of the test model in RT (open intake) and SPT with normal track condition.

In waterjet system performance analysis for WST and BPT, the inflow condition, i.e., $V_{1,@n=0}$, was well identified and E_1 was easy to estimate. For SPT, however, the ingested flow was perturbed by the hull owing to the blunt hull shape and momentum loss by severe free-surface wave generation, thus *w* should be introduced to determine U_A or $V_{1,@n=0}$. It is hard to measure U_A by the model test. A CFD analysis could be a good breakthrough for estimating E_1, but computation for such high-speed vessels or vehicles with dynamic attitude change is also a complicated problem (Lee and Rhee, 2015).

Figure 13 shows comparison of K_q in SPT and WST. For WST, K_q at J_A was derived and presented. As discussed in BPT results of Figure 10 (b), K_q increased, as the waterjets worked in favorable condition to produce more flow rate than WST.

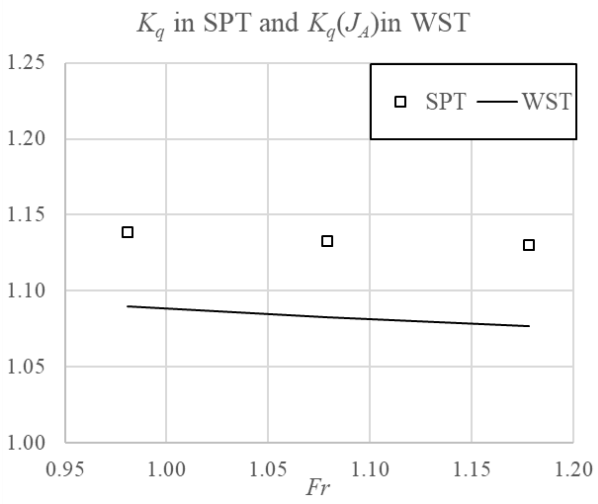

Figure 13. Comparison of K_q in WST and SPT

Figure 14 shows waterjet-hull interactions, η_{int}, and net propulsive efficiency, η_D. In the powering analysis of the conventional vessel, the propulsor-hull interaction is defined as the hull efficiency (η_H) and relative rotational efficiency (η_R), and η_{int} in the present study could be understood in the same manner. Like $\eta_H = (1 - t)/(1 - w)$, η_{int} increased when *t* decreased in high *Fr*, resulting in increased η_D.

Figure 15 shows the waterjet performance in SPT. For comparison, WST results at J_A were also presented. η_{pump} was similar to that in WST. η_{duct} in SPT was greater than that in WST owing to increased flow rate, in the same manner as BPT. The flow rate also affected η_I. V_6 in SPT was larger than that in WST, thus JVR reduced. It resulted in decrease of η_I.

It is noteworthy that η_{jet} hardly changed in SPT. Although the flow rate increased in SPT to produce larger momentum flux at the nozzle end, C_{p6} degraded and the net thrust did not increase. As a result, η_{net} assessed from SPT results was almost same to η_O at J_A. It implied that the net performance of the waterjet could be estimated from WST, if *w* was correctly assessed.

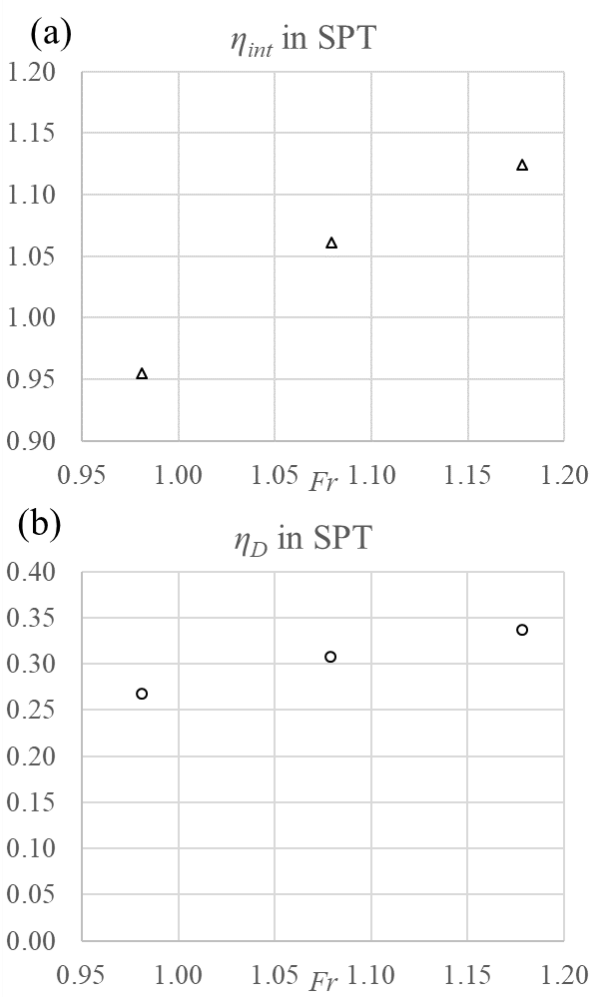

Figure 14. Waterjet-hull interaction: (a) η_{int} and (d) η_D

5 CONCLUSIONS

Propulsive performance of waterjet-propelled amphibious vehicle was analyzed by RT, WST, BPT, and SPT in a towing tank. The efficiency of energy conversion by waterjet system components were investigated, and study on hull-waterjet interaction was followed.

Based on the flow rate estimation, waterjet system performance in WST, BPT, and SPT was examined. In BPT and SPT, the flow rate increased by the pressure drop at the nozzle end. Such increased flow rate caused lower ideal jet efficiency in SPT than WST, but the negative pressure at the nozzle end in SPT made the jet efficiency similar to that in WST.

The most significant propulsion characteristic in SPT was the exposure of the transom, while massive flow separation was observed behind the transom in RT. It caused positive thrust deduction in high *Fr*. the quasi propulsive efficiency increased for larger *Fr*.

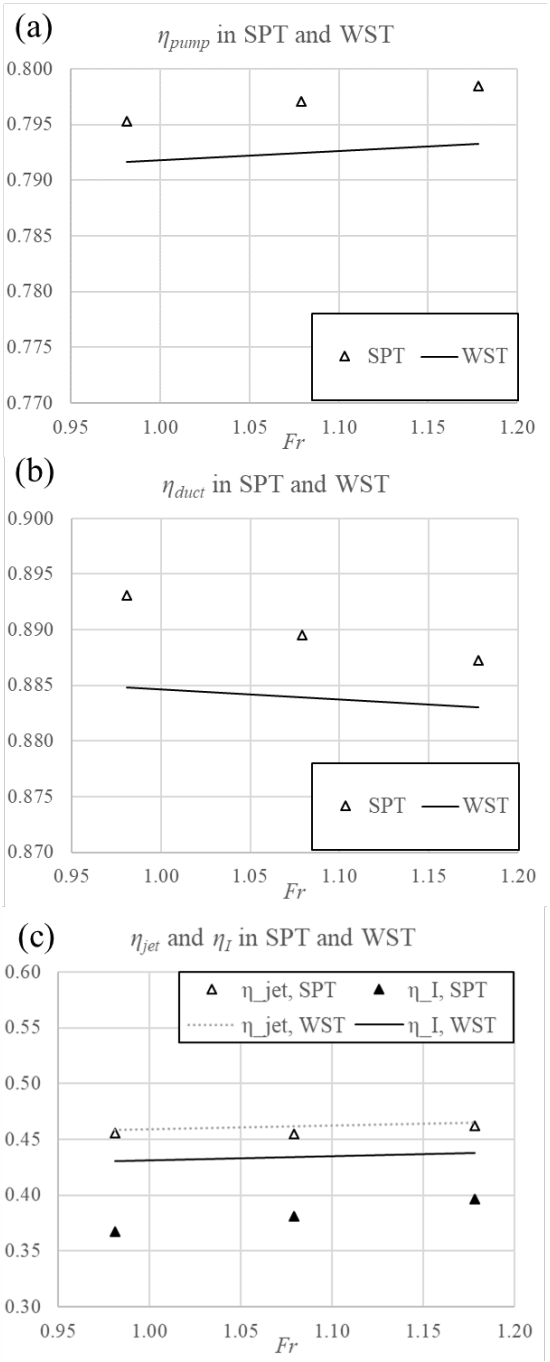

Figure 15. Waterjet system performance in SPT and WST at JA: (a) η_{pump}, (b) η_{duct}, and (c) η_{jet} and η_I

ACKNOWLEDGMENT

The research was supported by the Agency for Defense Development, and the Institute of Engineering Research at Seoul National University provided research facilities for this work.

REFERENCES

Allison, J. L., 1993. Marine Waterjet Propulsion, The Society of Naval Architects and Marine Engineers Transactions, Vol. 101, pp. 275-335.

ASME, 2005. Test Uncertainty. ASME Performance Test Code 19.1-2005, The American Society of Mechanical Engineers, New York, NY.

ITTC, 1996. Report of the Waterjets Group. Final Report and Recommendations to the 21st ITTC, International Towing Tank Conference, September 15 – 21, 1996, Trondheim, Norway

ITTC, 2011. Waterjet Propulsive Performance prediction. ITTC Quality System Manual Recommended Procedures and Guidelines. 7.5-02-05-03.1, International Towing Tank Conference, August 28 – September 3, 2011, Rio de Janeiro, Brazil

ITTC, 2017. Waterjet System Performance. ITTC Quality System Manual Recommended Procedures and Guidelines. 7.5-02-05-03.2, International Towing Tank Conference, September 17 – 22, Wuxi, China

Jung, U. H., Kim, M.-C., Chun, H.-H., and Lee, S.-H., 2009. Study on the Performance of Waterjet Propulsion System for 180 Ton Class Fishing Guard Ship. Journal of the Society of Naval Architects of Korea, Vol. 46, No. 2, pp. 127-135.

Kim, M.-C., Chun, H.-H., Kim, H. Y., Park, W. K., and Jung, U. H., 2009. Comparison of Waterjet Performance in Tracked Vehicles by Impeller Diameter. Ocean Engineering, Vol. 36, No. 17, pp. 1438-1445.

Lee, H. B. and Rhee, S. H., 2015. A Dynamic Interface Compression Method for VOF Simulations of High-Speed Planing Watercraft. Journal of Mechanical Science and Technology, Vol. 29, No. 5, pp. 1849-1857.

Lee, S.-J., Lee, T.-I., Lee, J.-J., Nam, W., and Suh, J.-C., 2017. Hydrodynamic Characteristics of a Hydrofoil-assisted Amphibious Vehicle. Journal of Ship Research, Vol. 61, No. 1, pp. 15-22.

Seo, J., Lee, S.-J., Han, B., and Rhee, S. H., 2016. Influence of Design Parameter Variations for Propeller-Boss-Cap-Fins on Hub Vortex Reduction. Journal of Ship Research, Vol. 60, No. 6, pp. 23-21